Journal of Medicinal Chemistry

Article

A New Approach of Mitigating CYP3A4 Induction Led to the Discovery of Potent Hepatitis B Virus (HBV) Capsid Inhibitor with Optimal ADMET Profiles

Xianfeng Lin, Houguang Shi, Weixing Zhang, Zongxing Qiu, Zheng Zhou, Fabian Dey, Sheng Zhong, Hongxia Qiu, Jianxun Xie, Xue Zhou, Guang Yang, Guozhi Tang, Hong C Shen, and Wei Zhu

J. Med. Chem., **Just Accepted Manuscript** • DOI: 10.1021/acs.jmedchem.9b01421 • Publication Date (Web): 05 Nov 2019

A New Approach of Mitigating CYP3A4 Induction Led to the Discovery of Potent Hepatitis B Virus (HBV) Capsid Inhibitor with Optimal ADMET Profiles

Xianfeng Lin,[&,†,§] Houguang Shi,[&,†,§] Weixing Zhang,[†,§] Zongxing Qiu,[†,§] Zheng Zhou, [†,‖] Fabian Dey, [‡, ‖] Sheng Zhong, [†,⊥] Hongxia Qiu,[†,⊥] Jianxun Xie, [†,⊥] Xue Zhou,[†,#] Guang Yang,[†,#] Guozhi Tang,[†,§] Hong C. Shen,[*,†,§] and Wei Zhu [*,†,§]

[†]Roche Innovation Center Shanghai, [‡]Roche Innovation Center Basel, [§]Medicinal Chemistry, [‖]Lead Discovery, [⊥]Pharmaceutical Sciences, [#]Discovery Virology, Roche Pharma Research and Early Development, Bldg 5, 720 Cailun Road, Shanghai 201203, China

[&]These two authors contributed equally to this work.

Abstract—Described herein is a new approach to mitigate CYP3A4 induction. In this unconventional approach, a fine-tuning of the dihedral angle between the C2 phenyl and the dihydropyrimidine core of the heteroaryldihydropyrimidine (HAP) class of capsid inhibitors successfully altered the structure-activity-relationships (SARs) of the unwanted CYP3A4 induction and the desired HBV capsid inhibition to more favorable values. This eventually led to the discovery of a new capsid inhibitor with significantly reduced CYP3A4 induction, excellent anti-HBV activity, favorable pre-clinical PK/PD profiles and no early safety flags.

Keywords— HBV, capsid inhibitor, HAP, CYP3A4 induction, PXR, dihedral angle, liver-to-plasma ratio, hydrodynamic injection (HDI) mouse model.

Introduction.

Hepatitis B virus (HBV), which chronically infects approximately 240 million people worldwide, is an important causative agent of liver fibrosis, cirrhosis and cancer.[1] Despite widespread implementation of the vaccination program, HBV infection remains a global health burden. However, the current standard of care (SoC), namely interferon and nucleos(t)ide analogues, cannot lead to a substantial HBV functional cure rate (typically much less than 10%), defined by the complete loss of HBV surface antigen (HBsAg) after a finite treatment period. It is also known that SoCs can be associated with either viral resistance or side effects.[2] Consequently, there has been a great demand in the discovery and development of non-nucleos(t)ide, direct-acting anti-HBV drugs with novel mechanism of action in order to improve disease cure rate, as a standalone therapy, or more likely, in combination with other antiviral agents.[3, 4]

The HBV core protein plays critical roles in the HBV lifecycle, with the most prominent one as the essential component of the nucleocapsid.[5] The core protein is conserved across all HBV genotypes and is thus considered as an attractive target for small molecule intervention. We previously reported a new HAP class of core protein inhibitors represented by **1** (HAP_R01) and **2** (HAP_R10), as shown in **Table 1**.[6] These compounds prevented the HBV core proteins from assembling into a normal nucleocapsid. The misassembled nucleocapsid was presumably subsequently degraded through the host proteasome pathway, resulting in the interruption of HBV replication.[5] The lead compound **2** demonstrated good *in vitro* and *in vivo* anti-HBV activity, favorable pre-clinical PK and early safety profiles. However, further development of compound **2** was hampered due to its strong CYP3A4 enzyme induction observed in human hepatocytes, which was later confirmed in the phase I clinical trial with healthy volunteers (unpublished).

The induction of CYP3A4 enzyme represents a significant clinical issue because CYP3A4 is involved in the metabolism of more than 50% of marketed drugs.[7] Specifically, CYP3A4 induction can lead to the reduction of therapeutic efficacy of a co-medication or the CYP3A4 inducer itself (a phenomenon known as auto-induction if the inducer itself is metabolized by CYP3A4). The induction of CYP3A4 enzyme can occur through several mechanisms, with the predominant one occurring through the activation of pregnane X receptor (PXR), a nuclear hormone receptor.[8] In the human PXR transactivation assay, both compounds **1** and **2** were found to be strong PXR activators, indicating PXR activation as the mechanism of CYP3A4 induction for this chemical class of capsid inhibitors. Several crystal structures of the human PXR ligand binding domain (LBD) complexed with structurally diversified PXR activators were reported, which revealed an unusually large and flexible binding pocket.[8, 9] A plausible pharmacophore model of PXR activators was proposed, which comprised one H-bond acceptor and at least two flanking hydrophobic groups, in particular aromatic groups.[8] The structure of the HAP class of capsid inhibitors represented by compound **1** and **2** coincidently contains all the pharmacophore elements favorable for hPXR binding, in which the C2 thiazoyl and the C4 phenyl play the part of hydrophobic groups and the nitrogen of the dihydropyrimidine or the carbonyl oxygen of the C5 methyl ester accounts for the key H-bonding interaction with PXR, thus potentially explaining the strong CYP3A4 induction effect observed for both compound **1** and **2**. The well adopted strategies to reduce hPXR activation include: (1) introducing polar substituent to the lipophilic group to destabilize the hydrophobic interactions; (2) removing the central H-bond acceptor.[8, 9] However, from the co-crystal structure of Cp149 Y132A mutant hexamer in complex with **1** (5WRE) (Figure 1a), both the C2 thiazoyl and the C4 phenyl were located in hydrophobic pockets, where introduction of polar substituent would essentially lead to a loss of binding affinity to core proteins.

Moreover, the removal of potential H-bond acceptors, e.g. replacing the dihydropyrimidine with dihydropyridine or C5 ester with triflouromethyl, led to a complete loss of anti-HBV activity. In this manuscript, we report a new approach to mitigate hPXR activation, which culminated with the discovery of a new capsid inhibitor with significantly reduced CYP3A4 induction, excellent anti-HBV activity, favorable pre-clinical PK/PD profiles, and no early safety flags.

Results and Discussion.

Working Hypothesis. In theory, when a ligand binds to its targeted protein, the closer the binding conformation is to its lowest energy conformation in water, the higher binding affinity it could exert. In the crystal structure of Cp149 Y132A in complex with compound **1** (5WRE), compound **1** binds to core proteins in a conformation where the C4 phenyl is nearly perpendicular to the dihydropyrimidine plane with a dihedral angle of -64.3° (Figure 1a).[6] This is almost identical to the conformation observed in the single crystal structure of compound **1a** (the core structure of compound **1**), where a dihedral angle of -64.5° is observed (Figure 1b and 1c) except for an 180° flip of the C4 phenyl ring in the co-crystal structure (the –Cl substituent will clash with the residues forming the cap if it orients as that in the co-crystal structure of **1a**).[6] Interestingly, in the CSD five out of the seven total related small molecule crystal structures (codes: 002548, 002919, 002920, FAGDAS, FAGDEW) show a similar conformation as observed in the protein/ligand crystal structure with dihedrals in the range between -62.3 and -88.5°.[10] The remaining two (codes 200608 and HAYPOP) have the phenyl flipped with the chlorine above the dihydropyrimidine plane and the ester flipped by 180° as well.[10] The concordance of the dihedral angles between C4 phenyl and dihydropyrimidine plane in water and in the binding pocket could nicely explain the high binding affinity of compound **1** to core proteins, and thus its strong anti-HBV activity.

Likewise, it was hypothesized that the strong CYP3A4 induction of compound **1** might also be ascribed to its favorable binding to hPXR LBD in this conformation.

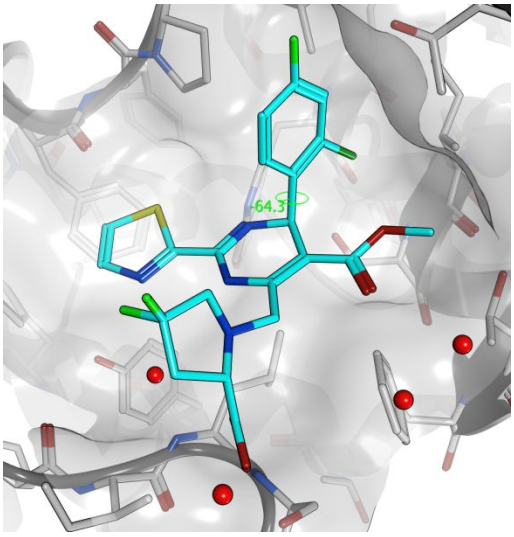

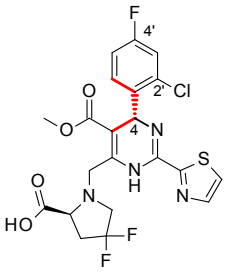

1 (HAP_R01)

Figure 1a: Crystal structure of Cp149 Y132A in complex with compound **1** (PDB code 5WRE). Compound **1** is shown in stick with cyan carbons. The molecular surface of the protein is shown in grey in the vicinity of the ligand. The core protein monomer forming the top of the binding pocket is omitted for clarity. The dihedral angle constituted by the bonds labelled in red in the schematic representation was -64.3° in the co-crystal structure.

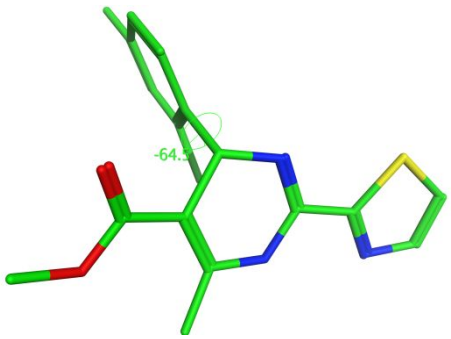

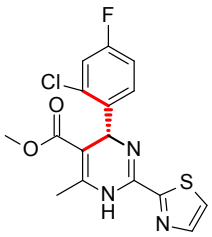

1a

Figure 1b: X-ray of **1a**. Compound **1a** was shown stick with the cyan carbons. The dihedral angle constituted by the bonds labelled in red in the schematic representation was -64.5°.

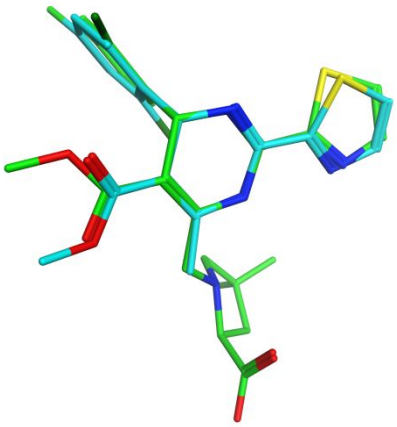

Figure 1c: Overlay of **1** (cyan) and **1a** (green).

As evident in the binding pocket (Figure 1a), there is still a bit of room around the C4 phenyl of compound **1** to allow it to move slightly around the C–C bond connecting to the dihydropyrimidine core. As such, the SAR of capsid inhibition might tolerate small changes of the dihedral angle between the C4 phenyl and the dihydropyrimidine plane. The medicinal chemistry efforts were thus focused on the modulation of this dihedral angle in order to separate SARs of CYP3A4 induction and capsid inhibition.

CYP3A4 Induction SAR. The 2'-substituent of C4 phenyl of compound **1** was assumed to be crucial in determining the dihedral angle between the C4 phenyl and the dihydropyrimidine plane. In the presence of an ester at the C5 position, the smaller the 2'-substituent, the smaller the dihedral angle will likely be inferred from modelling results (*vide infra*). As such, we set out to explore smaller substituents than –Cl, e.g. –H and –F.

The selected compounds were evaluated for their ability to induce CYP3A4 mRNA using the cryopreserved primary human hepatocytes. The induction was determined in cells exposed to

the individual compounds at a concentration of 10 μM by measuring CYP3A4 mRNA levels, in comparison with the positive control rifampicin (RIF) at the same concentration. The choice of 10 μM is for detection of induction signals as much as possible. An increase in CYP3A4 mRNA contents that was >40% of the level stimulated by rifampicin was clearly considered as a risk for induction in clinic based on internal experience and FDA guidance.[11]

Table 1: Data of anti-HBV EC_{50} and CYP3A4 induction of compound **1**–**20**.

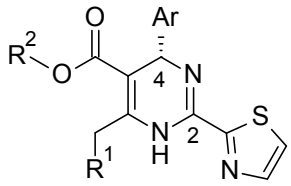

ID	Ar	R^1	R^2	EC_{50} (μM)[a]	CC_{50} (μM)[b]	CYP3A4 induction(%)[c]
1	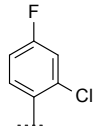	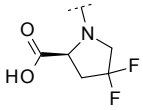	Methyl	0.003	65	109
2	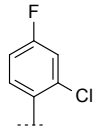	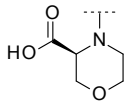	Methyl	0.003	> 100	111
3	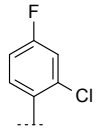	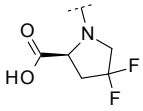	Ethyl	0.010	> 100	123
4	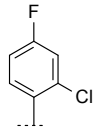	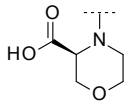	Ethyl	0.002	> 100	173

5	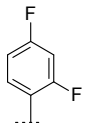	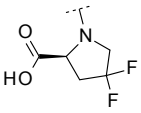	Methyl	- [d]	> 100	96
6	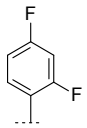	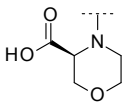	Ethyl	0.014	> 100	135
7	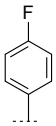	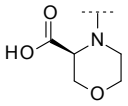	Ethyl	0.015	62	85
8	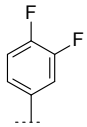	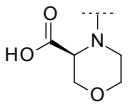	Ethyl	0.011	> 100	41
9a-c	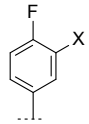 **X = Cl / Br / CN**	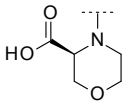	Ethyl	> 1	- [d]	- [d]
10	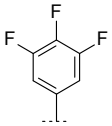	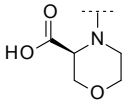	Ethyl	0.018	> 100	72
11	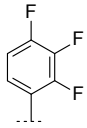	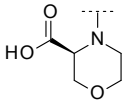	Ethyl	0.005	49	105
12	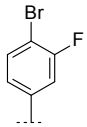	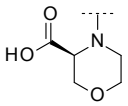	Ethyl	0.003	14	73
13	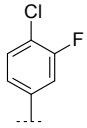	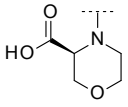	Ethyl	0.002	24	- [d]

14	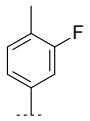	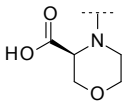	Ethyl	0.005	85	40
15	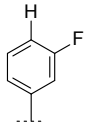	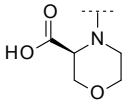	Ethyl	0.015	69	94
16	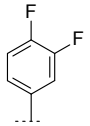	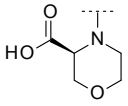	Methyl	0.046	> 100	36
17	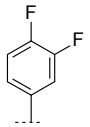	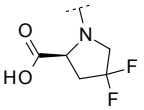	Methyl	0.022	56	52
18	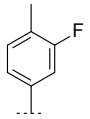	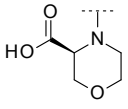	Methyl	0.028	> 100	- [d]
19	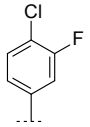	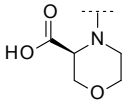	Methyl	0.01	> 100	25
20	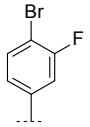	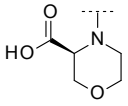	Methyl	0.01	76	26

[a] EC_{50} is the mean value for reduction of HBV DNA by 50% in HepG.2.2.15 cells. Experiments were run in duplicate, with variation < 15%. [b] CC_{50} is the mean value for cytotoxicity to HepDE19 cells. Experiments were in duplicate runs with variation < 15%. [c] mRNA level of CYP3A4 in percentage to that of rifampicin with compound treatment at 10μM. [d] Not determined.

As seen in Table 1, the 2'–F analogues **5** and **6** showed slightly reduced CYP3A4 induction compared to the 2'–Cl analogues **1** and **4**. The smaller 2'–H analogue **7** exhibited more

pronounced effect on reducing CYP3A4 induction with a value of 85% (**7** vs **4**) while still maintaining potent anti-HBV activity with an EC_{50} of 15 nM in HepG2.2.15 cells, which boosted our confidence in the exploration of this novel approach to reduce CYP3A4 induction.

With the preliminary success, we next set out to explore the effect of 3'–substituent on CYP3A4 induction. However, the effect on core protein binding was uncertain though there was a bit of room in the binding pocket. As such, we prepared the –CN, –F, –Cl, –Br substituted analogues at the 3'-position. From the SAR results, the substituents with a Van der Walla radii larger than –F were not tolerated in the capsid binding pocket, which led to a significant loss of anti-HBV activity (> 1 μM for all 3 analogues, Examples **9a-c**). However, the 3',4'-difluoro substituted analogue **8** maintained potent anti-HBV activity with an EC_{50} of 11 nM. More importantly it demonstrated an increased selectivity of anti-HBV activity *vs* CYP3A4 induction with the latter decreased to 41% of rifampicin (an average of >3 tests). Subsequently, we synthesized the 3',4',5'-trifluoro substituted analogue **10**, which, however, displayed a decrease of anti-HBV activity and an elevation of CYP3A4 induction. The introduction of one additional –F substituent at the 2'-position could further improve anti-HBV activity with an EC_{50} of 5 nM but at the cost of the increased CYP3A4 induction (Example **11**).

In order to further increase the selectivity of anti-HBV activity *vs* CYP3A4 induction, the substituent at the 4'-position was explored. From our previous SAR findings, we knew that the 4'–F of C4 phenyl could be successfully replaced with –Me, –Cl and –Br with comparable or even better anti-HBV activity.[6] Indeed, all three analogues (Examples **12**–**14**) displayed improved anti-HBV activity in the single digit nM range. Regarding CYP3A4 induction potential, compound **12** showed a value of 73% relative to rifampicin. However, considering its cytotoxicity profile (CC_{50} is 14 μM in HepDE19 cells), this result may not accurately reflect its induction potential in human

hepatocytes as cytotoxicity can affect CYP3A4 induction readout also at the tested concentration of 10 μM. Compound **13** also showed an unfavorable CC_{50} of 24 μM. The 4'–Me analogue **14** has potent anti-HBV EC_{50} of 5 nM, good CC_{50} of 85 μM and similar CYP3A4 induction level (40% relative to RIF) to compound **8**. The 4'–H analogue **15**, however, demonstrated an increased CYP3A4 induction potential (94% relative to RIF) albeit a similar anti-HBV EC_{50} to compound **8**.

Both analogues **8** and **14** demonstrated reduced CYP3A4 induction at a level around 40% relative to RIF, which met our preliminary goal. In order to minimize the concerns of DDI and auto induction in clinical use, we were keen to explore whether the CYP3A4 induction could be further reduced for this HAP chemical series. By comparing the C5 methyl ester to C5 ethyl ester analogues (**1** *vs* **3**, and **2** *vs* **4**), it was clear that the methyl ester analogues had lower potential of CYP3A4 induction likely due to their reduced lipophilicity.[12] As such, the corresponding C5 methyl ester analogues **16**–**20** were synthesized and the CYP3A4 induction data is summarized in **Table 1**. Indeed, they all demonstrated reduced CYP3A4 induction in human hepatocytes as compared to their corresponding ethyl ester analogues. As observed in previous SAR, they also showed decreased anti-HBV activity compared to the ethyl ester analogues, of which the 4'–Cl and 4'–Br analogues **19** and **20**, however, still displayed potent anti-HBV activity. Compound **19** was the most interesting one with an anti-HBV EC_{50} of 10 nM, a high CC_{50} of >100 μM and a low CYP3A4 induction value of 25%.

CYP3A4, CYP1A2 and CYP2B6 Induction Assessments of 19. With a low CYP3A4 induction potential at 10 μM, compound **19** was further tested in human hepatocytes for its induction potentials in a dose dependent manner for various CYP enzymes including CYP3A4, 1A2 and 2B6. As seen in Table 2, compound **19** showed dose dependent decrease of CYP3A4

induction from 10 to 0.1 μM (25% at 10 μM, 7.5% at 1 μM and 2% at 0.1 μM), which indicated indeed a low risk of DDI and auto-induction in clinical use. In contrast, compound **2** showed CYP3A4 inductions of 111%, 83% and 22% of rifampicin at 10, 1 and 0.1 μM, respectively. Moreover, compound **19** had neither CYP1A2 nor CYP2B6 induction liabilities as determined by the changes of individual mRNAs compared with that of corresponding positive controls (<40% was accepted as a low risk of induction).

Table 2: Induction data of **19** on CYP3A4, CYP1A2 and CYP2B6 mRNAs.

Enzyme subtype	Concentrations (μM)	% of positive control
CYP3A4[a]	0.1	2
	1	7.5
	10	25
CYP1A2[b]	0.1	1.0
	1	0.9
	10	1.7
CYP2B6[c]	0.1	1.3
	1	1.5
	10	1.4

[a] Data was reported as CYP3A4 mRNA change with the treatment of **19** in percentage to that of rifampicin at 10μM. [b] Data was reported as CYP1A2 mRNA change with the treatment of **19** in percentage to that of omeprazole at 10μM. [c] Data was reported as CYP2B6 mRNA change with the treatment of **19** in percentage to that of phenobarbital at 10μM.

Chemistry. The synthetic route of preparing this new series of 3',4'-disubstituted C4 phenyl HAP analogues was shown in Scheme 1. As exemplified by the synthesis of compound **19**, a three-component condensation reaction of methyl acetoacetate, 3-fluoro-4-chlorobenzaldehyde and thiazole-2-carboxamidine afforded the key intermediate dihydropyrimidine **19a** as a racemic mixture. An SFC (supercritical fluid chromatography) chiral separation of **19a** afforded two enantiomerically pure intermediates, of which (*S*)-**19a** was determined as the desired enantiomer by X-ray diffraction study. (*S*)-**19a** was then reacted with NBS to give bromide **19b**, which was finally coupled with (3*S*)-morpholine-3-carboxylic acid to provide **19** as a single isomer after HPLC purification.

Scheme 1: Preparation of compound 19

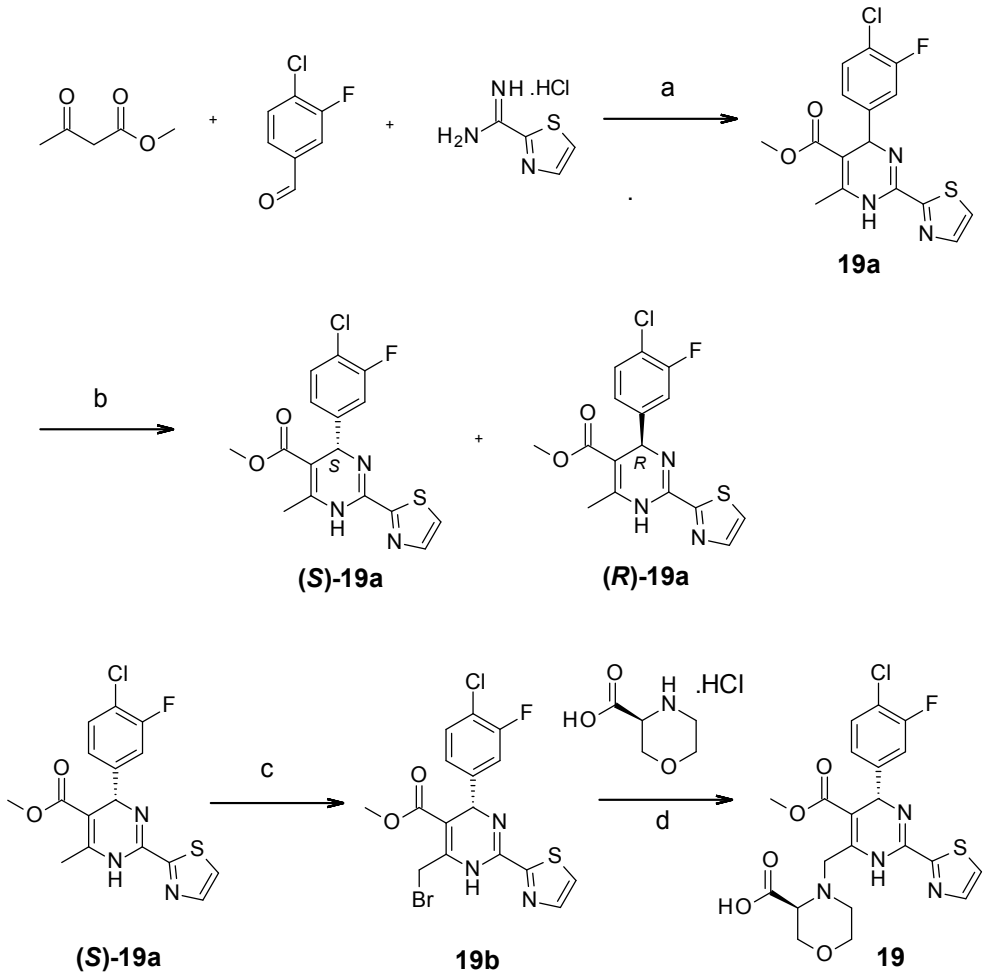

Reagents and conditions: (a) *i*-PrOH, HOAc, piperidine, 48 °C, 2 hours; followed by the addition of thiazole-2-carboxamidine, then 90 °C, 3 hours, 52%; (b) SFC chiral separation; (c) NBS, CCl_4, r.t., 1 hr, 44%; (d) DIPEA, DCM, ca. 1 hr, 57%.

Putative Explanation of the Reduced CYP3A4 Induction of 19. In order to prove that the 3',4'-disubstituted C4 phenyl analogues such as compound **19** indeed has a smaller dihedral angle between C4 phenyl and dihydropyrimidine plane than that of 2',4'-disubstituted C4 phenyl HAP analogues, we solved the single crystal structure of intermediate **(*S*)-19a**. Indeed, as shown in **Figure 3**, compound **(*S*)-19a** has a much smaller dihedral angle of 1.3° than that of compound **1a** (64.5°) (**Figure 2a** and **2b**). Interestingly, with this drastic conformation change, **(*S*)-19a** shows

an opposite optical rotation to **1a**, where **(*S*)-19a** has $[\alpha]_d^{20}$ of +50°, while **1a** has $[\alpha]_d^{20}$ of -55°. However, in the absence of any structural information on the binding of these compounds to hPXR, it remains speculative to ascribe the decreased CYP3A4 induction to the decreased dihedral angle though this dihedral angle change had a consistent and pronounced effect on hPXR activation. Two plausible explanations were proposed. On one hand, the preferable conformation of **19** in water with a small dihedral angle between C4 phenyl and the dihydropyrimidine core may fit poorly or lead to enthalpy penalty if the C4 phenyl has to be oriented to the conformation of a larger dihedral angle in the binding pocket of hPXR LBD. On the other hand, the nearly planar orientation of the C4 phenyl to the dihydropyrimidine plane might prevent either the 3-N of dihydropyrimidine or the carbonyl of C5 ester from forming a favorable hydrogen bonding interaction with the corresponding residues of hPXR, e.g. Ser247 or His407 as described in the literature.[8]

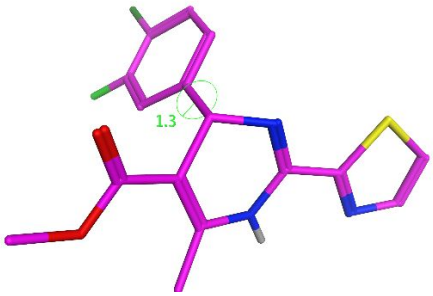

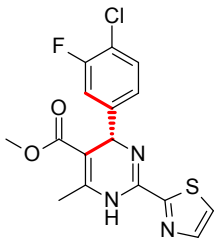

(*S*)-19a

Figure 2a: X-ray of **(*S*)-19a**. Compound **(*S*)-19a** was shown as ball and stick with the colour of carbon in cyan. The dihedral angle consisted by the bonds labelled in red in the schematic representation was 1.3°.

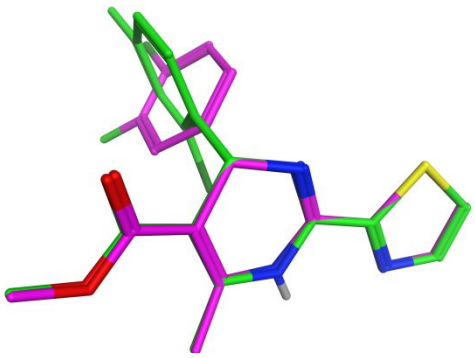

Figure 2b: Overlay of **1a** (green) and **(s)-19a** (purple).

ADMET and Preclinical PK/PD Studies of 19. With potent ant-HBV EC_{50}, higher CC_{50} and low CYP enzymes induction potential, **19** was further profiled in ADMET and pre-clinical PK/PD studies in order to evaluate its potential for further development. The physicochemical and ADME data were summarized in **Table 3**. Compound **19** had a LogD of 0.38 and two pKa values of 1.8 and 5.9, respectively. The ionizable carboxylic acid group of compound **19** offered the advantage of a high solubility of >666 µg/mL. Moreover, compound **19** showed good permeability under the conditions of the PAMPA assay at pH 6.5. This compound displayed a low human hepatic clearance and a moderate mouse hepatic clearance. Incubation in human hepatocytes revealed that the unchanged parent was the major form with a minor portion of a phase II metabolite as a result of glucuronide conjugation of the carboxylic acid group (the acylglucuronide reactivity was assessed low). Compound **19** also demonstrated a sufficient free fraction of 3.1% and 4.0% in human and mouse plasmas, respectively.

Table 3: Physicochemical, ADME and PK properties of **19**.

Physicochemical properties	
LogD[a]:	0.38
pKa[b] (acid/base):	1.8/5.9
ADME properties	

Lysa[c] (μg/mL):		>631
PAMPA[d] (10^{-6} cm/s):		2.4
Human/Mouse Hep_CL (mL min^{-1} kg^{-1})[e]:		3.6/48.6
PPB (human/mouse)[f]:		3.1/4.0
Mouse SDPK profiles[g]		
Plasma	$t_{1/2}$ (IV,H):	2.3
	V_{ss} (IV, L/kg):	2.7
	CL (IV) (mL min^{-1} kg^{-1}):	40.9
	C_{max} (PO, μg/L):	254
	$AUC_{(0-\infty)}$ (IV, μg/L*hr):	408
	$AUC_{(0-\infty)}$ (PO, μg/L*hr):	527
	F (%):	43.1
Liver	$AUC_{(0-\infty)}$ (PO, μg/L*hr):	19985
$AUC_{(0-\infty),\ liver}/AUC_{(0-\infty),\ plasma}$ (PO)		38

[a] Apparent partition coefficients at pH 7.4. [b] Ionization constant. [c] Lyophilisation solubility assay (LYSA) (μg/mL). [d] Parallel Artificial Membrane Permeability Assay (10^{-6} cm/s). [e] Predicted hepatic clearance obtained with human and mouse hepatocytes (mL min^{-1} kg^{-1}). [f] Plasma protein binding assay (% unbound fraction, average of 3 tests). [g] The single-dose pharmacokinetics (SDPK) study of **19** was carried out in mice as indicated according to the standard procedures (IV: 1 mg/kg; PO.: 3 mg/kg). Major parameters, including plasma clearance (*Cl*), volume of distribution at steady state (V_{ss}), $T_{1/2}$ (i.v.), Maximal concentration (C_{max}), area under the curve (AUC), and oral bioavailability (*F*) are reported.

In mouse SDPK studies, compound **19** showed a moderate clearance similar to the *in vitro* prediction in mouse hepatocytes, a moderate half-life and oral bioavailability. Despite a relatively low oral exposure in plasma, **19** demonstrated a high liver exposure (liver-to-plasma exposure ratio was 38), which was a desirable property for HBV infection treatment as liver is the disease organ.

Supported by potent *in vitro* anti-HBV activity and favorable mouse PK profiles, compound **19** was assessed against HBV infection in the hydrodynamic injection (HDI) mouse

model.[13] In this study, female BALB/c mice were hydrodynamically injected with replication-competent HBV DNA plasmid through the tail vein. Twenty hours post plasmid injection, mice were orally dosed by blank vehicle, entecavir (ETV, 0.1 mg/kg, once daily as the positive control), or different doses (3 and 12 mg/kg per dose, twice daily) of compound **19** for 5 days. Plasma and liver samples were collected at the indicated time points for HBV DNA quantification by real-time quantitative polymerase chain reaction (qPCR). As shown in **Figure 3**, with treatment of compound **19**, HBV DNA copy numbers were rapidly and markedly reduced in plasma and were hardly detectable in liver tissues, demonstrating a strong anti-HBV effect of compound **19** upon oral administration. The maximum efficacy of compound **19** was comparable to the maximum efficacy of ETV in this model.

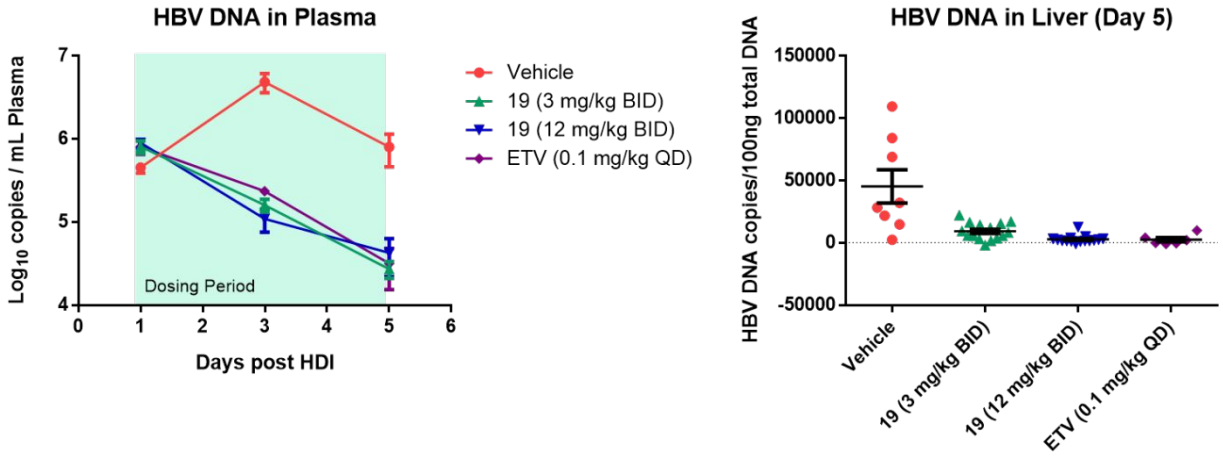

Figure 3: Levels of HBV DNA in plasma (A) and liver (B) of HBV HDI mice upon treatment with the vehicle control, ETV control, and compound **19**. Error bars indicate standard error of the mean.

Like its close analogue **2**, compound **19** was also clean in the following *in vitro* safety assessment including hERG, GSH (glutathione adduction), mutagenicity (Ames assay) and clastogenicity (micronucleus assay). The 5-day minitox study in rats showed sufficient safety

margin as defined by ratio of the plasma exposure (C_{max} and AUC) in rat at NOAEL (no observed adverse effect level) versus the exposure at a projected human efficacious dose, which all supported further development of **19**.

Conclusions.

In summary, we have described herein a novel approach to reduce CYP3A4 induction, which relied on a finely designed conformational change between two close analogues in the same chemical series. This seemingly unexpected finding might remind medicinal chemists of the importance of looking at the ligand in a 3D (3-dimensional) way (they may look very similar in 2D, but differ dramatically in 3D!). Plausible explanations of the conformation effect on CYP3A4 induction were provided also. However, given the promiscuous nature of the ligand-binding site of PXR which can accommodate structurally diverse small molecules in multiple ways, additional strategies have been identified to completely abolish hPXR binding while retaining anti-HBV activity in the HAP class of capsid inhibitors. Further research in this area will be reported in due course.

Experimental Section

Synthetic Chemistry General Comments. All of the intermediates were purified by silica gel chromatography using either a Biotage SP1 system or an ISCO CombiFlash chromatography instrument. All of the final compounds were purified by preparative HPLC (prep-HPLC) on a reversed-phase column using a Waters XBridge OBD Phenyl (30 mm × 100 mm, 5 μm) or OBD RP18 (30 mm × 100 mm, 5 μm) column under acidic conditions (A, 0.1% formic acid in H_2O; B, 0.1% formic acid in acetonitrile) or basic conditions (A, 0.1% ammonia in H_2O; B, acetonitrile). For SFC chiral separation, the intermediates were separated using a chiral column (Daicel

Chiralpak IC, 30 mm × 250 mm, 5 μm) on a Mettler Teledo SFC-Multigram system (solvent system of 95% CO_2 and 5% IPA (0.5% TEA in IPA), backpressure of 100 bar, UV detection at 254 nm). Optical rotation was measured using a Rudolph Autopol V automatic polarimeter at a wavelength of 589 nm. LC–MS spectra were obtained using a MicroMass Platform LC (Waters Alliance 2795-ZQ2000). NMR spectra were obtained using Bruker AVANCE 400 MHz spectrometer, operating at 400.13 MHz (^{1}H) and 100.62 MHz (^{13}C). ^{1}H NMR spectra were obtained using the single pulse zg30.^{13}C{^{1}H} NMR spectra were obtained using composite pulse zgpg30 for proton decoupling. The chemical shifts were referenced against internal TMS(^{1}H,^{13}C) and the coupling constants were calculated as a whole of H,H and H,F. All of the starting materials were obtained commercially. All of the final compounds had purities greater than 95% based upon HPLC, LC–MS and ^{1}H NMR analyses. All of the reported yields are for isolated products and are not optimized.

General Synthetic Procedure: exemplified by (3*S*)-4-[[(4*S*)-4-(4-chloro-3-fluoro-phenyl)-5-methoxycarbonyl-2-thiazol-2-yl-1,4-dihydropyrimidin-6-yl]methyl]morpholine-3-carboxylic acid (19).

To a stirred solution of 4-chloro-3-fluorobenzaldehyde (0.500 g, 0.32 mmol) and methyl acetoacetate (0.366 g, 3.2 mmol) in *i*-PrOH (6 mL) were added acetic acid (0.020 g, 0.034 mmol) and piperdine (0.027 g, 0.032 mmol) at 48 ^{o}C. The resulting mixture was stirred at 48 ^{o}C for two hours. Then thiazole-2-carboxamidine hydrochloride (0.516 g, crude, ca. 2.52 mmol) and triethylamine (0.318 g, 3.2 mmol) were added to the reaction mixture. The mixture was heated at 90 ^{o}C for three hours. After it was cooled to room temperature, the reaction mixture was concentrated and the residue was dissolved in ethyl acetate and washed with brine. The organic layer was dried over anhydrous Na_2SO_4. The solvent was removed and the residue was purified by

silica gel column chromatography (ethyl acetate/petroleum ether: 1/4 to 1/2) to afford methyl 4-(4-chloro-3-fluoro-phenyl)-6-methyl-2-thiazol-2-yl-1,4-dihydropyrimidine-5-carboxylate (Compound **19a**) as a yellow solid (600 mg, 52%). MS: calc'd (MH^+) 366, measured (MH^+) 366. ^1H NMR (MeOD-d_4, 400 MHz) δ ppm 7.96 (m, 1H), 7.77 (m, 1H), 7.42 (m, 1H), 7.18 (m, 2H), 5.69 (*br* s, 1H), 3.69 (s, 3H), 2.49 (s, 3H).

The racemic compound **19a** was subjected to SFC chiral separation. The desired (-)-enantiomer methyl (4*S*)-4-(4-chloro-3-fluoro-phenyl)-6-methyl-2-thiazol-2-yl-1,4-dihydropyrimidine-5-carboxylate (**(*S*)-19a**) has a relatively short retention time. The absolute stereochemistry of **(*S*)-19a** was determined by X-ray diffraction study (see supporting information). **(*S*)-19a**: $[\alpha]_D^{20}$ +50° (c 0.21 g/100 mL, MeOH).

To a stirred solution of compound **(*S*)-19a** (0.160 g, 0.44 mmol) in CCl_4 (5 mL) was added NBS (0.070 g, 0.39 mmol) in portions. After the reaction mixture was stirred at 70 °C for 3 hours, the solvent was removed *in vacuo* and the residue was purified by column chromatography to give methyl (4*S*)-6-(bromomethyl)-4-(4-chloro-3-fluoro-phenyl)-2-thiazol-2-yl-1,4-dihydropyrimidine-5-carboxylate (compound **19b**) as a yellow solid (0.086 g, 44%). MS: calc'd 445 (MH^+), measured 445 (MH^+).

To a stirred solution of compound **19b** (0.086 g, 0.19 mmol) and (3*S*)-morpholine-3-carboxylic acid hydrochloride salt (cas: 1187929-04-9, 0.042 g, 0.25 mmol) in dichloromethane (1 mL) was added dropwise DIPEA (0.13 mL, 0.77 mmol). The reaction mixture was stirred at room temperature until the disappearance of **19b**. The mixture was diluted with EtOAc (10 mL), washed successively with saturated aqueous NH_4Cl solution and brine. The organic layer was separated and dried over anhydrous Na_2SO_4. The solvent was concentrated *in vacuo* and the residue was purified by prep-HPLC to give (3*S*)-4-[[(4*S*)-4-(4-chloro-3-fluoro-phenyl)-5-methoxycarbonyl-2-

thiazol-2-yl-1,4-dihydropyrimidin-6-yl]methyl]morpholine-3-carboxylic acid (compound **19**) as a light yellow solid (0.055 mg, 57%). Melting point: 136.5 °C. MS: calc'd (MH^+) 495, measured (MH^+) 495. HRMS: calc'd (MH^+) 495.08997, measured (MH^+) 495.08958. ^{1}H NMR (DMSO-d6, 400 MHz) δ ppm 12.9–13.0 (m, 1H), 12.9–13.0 (m, 1H), 12.4–13.0 (m, 1H), 9.8–10.0 (m, 1H), 8.0–8.1 (m, 1H), 7.9–8.0 (m, 1H), 7.5–7.6 (m, 1H), 7.3–7.3 (m, 1H), 7.2–7.2 (m, 1H), 5.6–5.7 (m, 1H), 4.25 (*br* d, 1H, J = 17.6 Hz), 3.9–4.0 (m, 2H), 3.8–3.8 (m, 1H), 3.6–3.7 (m, 2H), 3.6–3.6 (m, 4H), 3.0–3.1 (m, 1H), 2.35 (*br* d, 1H, J = 12.1 Hz). ^{13}C NMR (DMSO-d_6, 400 MHz): δ ppm 172.8, 166.3, 162.4, 158.9, 156.4, 147.5, 146.7(d, $^2J_{CF}$=20 Hz, FC), 145.4, 144.2, 131.2, 125.3, 124.7 (d, $^3J_{CF}$=12 HZ, FC), 118.7, 118.6, 115.8, 115.6, 97.1, 69.4, 67.2, 61.9, 58.6, 54.8, 51.5, 48.5.

The following compounds are prepared in analogy to 19 from commercially available building blocks.

(*R*)-6-((*S*)-2-Carboxy-4,4-difluoro-pyrrolidin-1-ylmethyl)-4-(2-chloro-4-fluoro-phenyl)-2-thiazol-2-yl-1,4-dihydro-pyrimidine-5-carboxylic acid ethyl ester (3). MS: calc'd 529 (MH^+), exp 529 (MH^+). ^{1}H NMR (MeOD-d_4, 400 MHz): δ ppm 8.09 (d, J = 3.01 Hz, 1H), 8.02 (d, J = 3.01 Hz, 1H), 7.57 (dd, J = 8.78, 6.02 Hz, 1H), 7.32 (dd, J = 8.78,2.51 Hz, 1H), 7.16 (td, J = 8.41, 2.51 Hz, 1H), 6.25 (s, 1H), 4.53 (d, J = 16.06 Hz, 1H), 4.00–4.18 (m, 4H), 3.68 (q, J = 11.13 Hz, 1H), 3.20–3.30 (m,1H), 2.77–2.94 (m, 1H), 2.49–2.65 (m, 1H), 1.17 (t, J = 7.15 Hz, 3H).

(*S*)-4-[(*R*)-6-(2-Chloro-4-fluoro-phenyl)-5-ethoxycarbonyl-2-thiazol-2-yl-3,6-dihydro-pyrimidin-4-ylmethyl]-morpholine-3-carboxylic acid (4). MS: calc'd (MH^+) 509, measured (MH^+) 509. ^{1}H NMR (MeOD-d_4, 400 MHz): δ ppm 8.08 (d, J = 3.01 Hz, 1H), 8.01 (d, J = 3.01 Hz, 1H), 7.60 (dd, J = 8.53, 6.02 Hz, 1H), 7.31 (dd, J = 8.66,2.38 Hz, 1H), 7.15 (td, J = 8.34, 2.38 Hz, 1H), 6.26 (s, 1H), 4.88 (d, J = 16.31 Hz, 1H), 4.59 (d, J = 16.56 Hz, 1H), 4.26–4.33 (m, 1H),

4.22 (d, *J* = 4.02Hz, 2H), 4.11 (q, *J* = 6.94 Hz, 2H), 3.93–4.05 (m, 2H), 3.78 (ddd, *J* = 12.42, 8.28, 3.64 Hz, 1H), 3.27 (d, *J* = 13.05 Hz, 1H), 1.16 (t, *J* = 7.15 Hz, 3H).

(2*S*)-1-[[(4*R*)-4-(2,4-difluorophenyl)-5-methoxycarbonyl-2-thiazol-2-yl-1,4-dihydropyrimidin-6-yl]methyl]-4,4-difluoro-pyrrolidine-2-carboxylic acid (5). MS: calc'd 499 (MH^+), exp 499 (MH^+). ^{1}H NMR (MeOD-d_4, 400 MHz): δ ppm 8.14 (dd, *J* = 3.1, 12.9 Hz, 2H), 7.53 (dt, *J* = 6.5, 8.5 Hz, 1H), 7.0–7.1 (m, 2H), 6.04 (s, 1H), 4.54 (d, *J* = 16.1 Hz, 1H), 4.0–4.2 (m, 2H), 3.70 (s, 3H), 3.5–3.7 (m, 1H), 3.2–3.3 (m, 1H), 2.8–2.9 (m, 1H), 2.5–2.6 (m, 1H).

(*S*)-4-[(*R*)-6-(2,4-Difluoro-phenyl)-5-ethoxycarbonyl-2-thiazol-2-yl-3,6-dihydro-pyrimidin-4-ylmethyl]-morpholine-3-carboxylic acid (6). MS: calc'd 493 (MH^+), exp 493 (MH^+). ^{1}H NMR (MeOD-d_4, 400 MHz): δ ppm 7.98 (d, *J* = 2.8 Hz, 1H), 7.79 (d, *J* = 2.8 Hz, 1H), 7.50–7.36 (m, 1H), 7.04–6.87 (m, 2H), 6.02–5.93 (m, 1H), 4.38–4.19 (m, 2H), 4.17–4.00 (m, 4H), 3.97–3.78 (m, 3H), 3.58 (br. s., 1H), 2.71 (*br*. s., 1H), 1.19 (t, *J* = 7.0 Hz, 3H).

(*S*)-4-[(*S*)-5-Ethoxycarbonyl-6-(4-fluoro-phenyl)-2-thiazol-2-yl-3,6-dihydro-pyrimidin-4-ylmethyl]-morpholine-3-carboxylic acid (7). MS: calc'd 475 (MH^+), exp 475 (MH^+). ^{1}H NMR (MeOD-d_4, 400 MHz): δ ppm 8.00 (d, *J* = 3.0 Hz, 1H), 7.84 (d, *J* = 3.0 Hz, 1H), 7.41 (dd, *J* = 5.4, 8.7 Hz, 2H), 7.07 (t, *J* = 8.8 Hz, 2H), 5.71 (s, 1H), 4.58 (d, *J* = 16.1 Hz, 1H), 4.31 (br. s., 1H), 4.21–4.03 (m, 4H), 3.98–3.81 (m, 2H), 3.71 (br. s., 1H), 3.50 (dd, *J* = 1.6, 3.4 Hz, 1H), 2.85 (br. s., 1H), 1.23 (t, *J* = 7.2 Hz, 3H).

(*S*)-4-[(*S*)-6-(3,4-Difluoro-phenyl)-5-ethoxycarbonyl-2-thiazol-2-yl-3,6-dihydro-pyrimidin-4-ylmethyl]-morpholine-3-carboxylic acid (8). MS: calc'd 493 (MH^+), exp 493 (MH^+). ^{1}H NMR (MeOD-d_4, 400 MHz): δ ppm 8.00 (d, *J* = 3.26 Hz, 1H), 7.83 (d, *J* = 3.01 Hz, 1H), 7.14–7.31 (m, 3H), 5.71 (s, 1H), 4.54 (d, *J* = 17.07 Hz, 1H), 4.02–4.30 (m, 5H), 3.78–3.98 (m, 2H), 3.67 (t, *J* = 3.89 Hz, 1H), 3.41 (br. s., 1H), 2.70–2.86 (m, 1H), 1.24 (t, *J* = 7.15 Hz, 3H).

(*S*)-4-[(*S*)-5-Ethoxycarbonyl-2-thiazol-2-yl-6-(3,4,5-trifluoro-phenyl)-3,6-dihydro-pyrimidin-4-ylmethyl]-morpholine-3-carboxylic acid (10). MS: calc'd 511 (MH^+), exp 511 (MH^+). ^{1}H NMR (MeOD-d_4, 400 MHz): δ ppm 8.01 (d, *J* = 3.26 Hz, 1H), 7.83 (d, *J* = 3.26 Hz, 1H), 7.13 (dd, *J* = 8.66, 6.65 Hz, 2H), 5.72 (s, 1H), 4.55 (d, *J* = 17.32 Hz, 1H), 4.01–4.26 (m, 5H), 3.78–3.96 (m, 2H), 3.67 (t, *J* = 3.76 Hz, 1H), 3.35–3.47 (m, 1H), 2.61–2.79 (m, 1H), 1.25 (t, *J* = 7.03 Hz, 3H).

(*S*)-4-[(*R*)-5-Ethoxycarbonyl-2-thiazol-2-yl-6-(2,3,4-trifluoro-phenyl)-3,6-dihydro-pyrimidin-4-ylmethyl]-morpholine-3-carboxylic acid (11). MS: calc'd 511 (MH^+), exp 511 (MH^+). ^{1}H NMR (MeOD-d_4, 400 MHz): δ ppm 7.93–8.08 (m, 1H), 7.76–7.90 (m, 1H), 7.19–7.31 (m, 1H), 7.04–7.16 (m, 1H), 6.02 (br. s., 1H), 4.35–4.54 (m, 1H), 4.10 (d, *J* = 4.77 Hz, 4H), 3.79–3.97 (m, 2H), 3.56–3.70 (m, 1H), 2.61–2.81 (m, 1H), 1.09–1.30 (m, 3H).

(*S*)-4-[(*S*)-6-(4-Bromo-3-fluoro-phenyl)-5-ethoxycarbonyl-2-thiazol-2-yl-3,6-dihydro-pyrimidin-4-ylmethyl]-morpholine-3-carboxylic acid (12). MS: calc'd 553 (MH^+), exp 553 (MH^+). ^{1}H NMR (MeOD-d_4, 400 MHz): δ ppm 8.01 (d, *J* = 3.3 Hz, 1H), 7.83 (d, *J* = 3.0 Hz, 1H), 7.59 (dd, *J* = 7.3, 8.3 Hz, 1H), 7.22 (dd, *J* = 2.0, 9.8 Hz, 1H), 7.15 (dd, *J* = 2.0, 8.3 Hz, 1H), 5.73 (s, 1H), 4.53 (d, *J* = 16.8 Hz, 1H), 4.27–4.01 (m, 5H), 3.98–3.80 (m, 2H), 3.67 (*br*. s, 1H), 3.36 (d, *J* = 6.0 Hz, 1H), 2.73 (*br*. s., 1H), 1.24 (t, *J* = 7.2 Hz, 3H).

(*S*)-4-[(*S*)-6-(4-Chloro-3-fluoro-phenyl)-5-ethoxycarbonyl-2-thiazol-2-yl-3,6-dihydro-pyrimidin-4-ylmethyl]-morpholine-3-carboxylic acid (13). MS: calc'd (MH^+) 509, measured (MH^+) 509. ^{1}H NMR (MeOD-d_4, 400 MHz): δ ppm 8.06-8.04 (m, 1H), 7.97–7.95 (m, 1H), 7.46–7.42 (m, 1H), 7.25–7.20 (m, 2H), 5.73 (s, 1H), 4.25–4.09 (m, 5H), 3.95–3.81 (m, 3H), 3.75–3.61 (m, 3H), 1.25 (t, *J* = 7.2 Hz, 3H).

(*3S*)-4-[[(*4S*)-5-ethoxycarbonyl-4-(3-fluoro-4-methyl-phenyl)-2-thiazol-2-yl-1,4-

dihydropyrimidin-6-yl]methyl]morpholine-3-carboxylic acid (14). MS: calc'd (MH^+) 489, measured (MH^+) 489. ^{1}H NMR (MeOD-d_4, 400 MHz): δ ppm 8.00 (d, *J* = 3.0 Hz, 1H), 7.84 (d, *J* = 3.3 Hz, 1H), 7.16–7.26 (m, 1H), 6.95–7.13 (m, 2H), 5.69 (s, 1H), 4.46–4.71 (m, 1H), 4.21–4.38 (m, 1H), 4.03–4.22 (m, 4H), 3.78–3.97 (m, 2H), 3.60–3.75 (m, 1H), 3.38–3.54 (m, 1H), 2.69–2.94 (m, 1H), 2.24 (d, *J* = 1.5 Hz, 3H), 1.24 (t, *J* = 7.2 Hz, 3H).

(*S*)-4-[(*S*)-5-Ethoxycarbonyl-6-(3-fluoro-phenyl)-2-thiazol-2-yl-3,6-dihydro-pyrimidin-4-ylmethyl]-morpholine-3-carboxylic acid (15). MS: calc'd 475 (MH^+), exp 475 (MH^+). ^{1}H NMR (MeOD-d_4, 400 MHz): δ ppm 8.01 (d, *J* = 3.0 Hz, 1H), 7.83 (d, *J* = 3.3 Hz, 1H), 7.35 (dt, *J* = 6.0, 7.9 Hz, 1H), 7.22 (d, *J* = 7.5 Hz, 1H), 7.10 (td, *J* = 2.0, 9.9 Hz, 1H), 7.01 (dt, *J* = 2.0, 8.4 Hz, 1H), 5.74 (s, 1H), 4.53 (d, *J* = 14.1 Hz, 1H), 4.34–4.02 (m, 5H), 3.98–3.80 (m, 2H), 3.66 (*br*. s., 1H), 3.47–3.36 (m, 1H), 2.77 (*br*. s., 1H), 1.24 (t, *J* = 7.2 Hz, 3H).

(3*S*)-4-[[(4*S*)-4-(3,4-difluorophenyl)-5-methoxycarbonyl-2-thiazol-2-yl-1,4-dihydropyrimidin-6-yl]methyl]morpholine-3-carboxylic acid (16). MS: calc'd 499 (MH^+), exp 499 (MH^+). ^{1}H NMR (MeOD-d_4, 400 MHz): δ ppm 8.57 (s, 1H), 7.99 (d, *J* = 3.3 Hz, 1H), 7.75 (d, *J* = 3.1 Hz, 1H), 7.1–7.3 (m, 3H), 5.68 (s, 1H), 3.9–4.1 (m, 3H), 3.7–3.9 (m, 3H), 3.68 (s, 3H), 3.24 (dd, *J* = 3.5, 8.3 Hz, 1H), 2.97 (*br* d, *J* = 11.8 Hz, 1H), 2.48 (ddd, *J* = 3.3, 8.9, 11.8 Hz, 1H).

(2*S*)-1-[[(4*S*)-4-(3,4-difluorophenyl)-5-methoxycarbonyl-2-thiazol-2-yl-1,4-dihydropyrimidin-6-yl]methyl]-4,4-difluoro-pyrrolidine-2-carboxylic acid (17). MS: calc'd 479 (MH^+), exp 479 (MH^+). ^{1}H NMR (MeOD-d_4, 400 MHz): δ ppm 8.07 (d, *J* = 3.0 Hz, 1H), 7.98 (d, *J* = 3.0 Hz, 1H), 7.2–7.4 (m, 3H), 5.76 (s, 1H), 4.45 (d, *J* = 16.3 Hz, 1H), 4.22 (d, *J* = 16.3 Hz, 1H), 4.04 (t, *J* = 8.2 Hz, 1H), 3.71 (s, 3H), 3.6–3.7 (m, 1H), 3.2–3.3 (m, 1H), 2.84 (ddt, *J* = 8.9, 11.5, 14.9 Hz, 1H), 2.5–2.6 (m, 1H).

(*3S*)-4-[[(*4S*)-4-(3-fluoro-4-methyl-phenyl)-5-methoxycarbonyl-2-thiazol-2-yl-1,4-dihydropyrimidin-6-yl]methyl]morpholine-3-carboxylic acid (18). MS: calc'd (MH^+) 475, measured (MH^+) 475. ^{1}H NMR (MeOD-d_4, 400 MHz): δ ppm 8.00 (d, *J* = 3.0 Hz, 1H), 7.84 (d, *J* = 3.3 Hz, 1H), 7.15–7.26 (m, 1H), 6.97-7.12 (m, 2H), 5.69 (s, 1H), 4.47–4.67 (m, 1H), 4.23–4.34 (m, 1H), 4.01–4.19 (m, 2H), 3.81–3.98 (m, 2H), 3.64–3.73 (m, 1H), 3.40–3.54 (m, 1H), 2.71–2.94 (m, 1H), 2.24 (d, *J* = 1.5 Hz, 3H), 1.24 (t, *J* = 7.2 Hz, 3H).

(*3S*)-4-[[(*4S*)-4-(4-bromo-3-fluoro-phenyl)-5-methoxycarbonyl-2-thiazol-2-yl-1,4-dihydropyrimidin-6-yl]methyl]morpholine-3-carboxylic acid (20). MS: calc'd (MH^+) 539, measured (MH^+) 539. ^{1}H NMR (MeOD-d_4, 400 MHz): δ ppm 8.01 (d, *J* = 3.3 Hz, 1H), 7.84 (d, *J* = 3.0 Hz, 1H), 7.59 (dd, *J* = 8.3, 7.3 Hz, 1H), 7.09–7.28 (m, 2H), 5.73 (s, 1H), 4.44–4.70 (m, 1H), 4.02–4.30 (m, 3H), 3.77–3.96 (m, 2H), 3.71 (s, 3H), 3.36–3.47 (m, 2H), 2.64–2.91 (m, 1H).

Cells and culture conditions: HepG2.2.15 and HepDE19 are stably-transfected cell lines containing the HBV genome. Both cell lines are derived from the hepatoblastoma cell line Hep G2 (American Type Culture Collection, ATCC® HB-8065™) by the published procedures.[14, 15] Both cell lines were maintained in Dulbecco's modified Eagle's medium (DMEM)-F12 medium supplemented with 10% fetal bovine serum, 100 U/mL penicillin, 100 μg/mL streptomycin, and 0.5 mg/mL of G418. While HepG2.2.15 cells constitutively support HBV replication and production of virus particles, HepDE19 cells are inducible by tetracycline. Addition of 1μg/mL tetracycline in culture medium suppresses HBV replication in HepDE19 cells, whereas switching to tetracycline-free medium resumes this process.

Anti-HBV activity *in vitro*: HepG2.2.15 cells were seeded into 96-well plates (3×10^4 cells in 100 μL media per well) and incubated overnight at 37 ºC. The test compounds were serially half-log diluted in DMSO, then diluted 100 times in culture media. 100 μL of diluted compounds were

added into the plates to reach 0.5% final concentration of DMSO in every well. Five days after compound treatment, culture supernatant was collected for further analysis. For quantitative PCR detection of extracellular HBV DNA, 100 μL of culture supernatant was collected and processed in MagNA Pure 96 Nucleic Acid Purification System (Roche Applied Science) for viral DNA extraction. The extracted samples were subjected to HBV DNA quantification by qPCR. The effective compound concentration at which HBV replication is inhibited by 50% (EC_{50}) was determined.

Cytotoxicity assay: HepDE19 cells were seeded into 96-well plates (5×10^3 cells per well) and treated with compounds for CC_{50} determination. Five days after treatment, cell viability was measured by addition of 20 μL of CCK-8 reagent. Two hours after incubation at 37°C, the absorbance at wavelengths of 450 nm and 630 nm (OD_{450} and OD_{630}) was recorded by a plate reader. The concentration results in the death of 50% of the host cells (CC_{50}) of each compound were determined.

LYSA Solubility Assay. Samples are prepared in duplicate from 10 mM DMSO stock solution. After evaporation of DMSO with a centrifugal vacuum evaporator, compounds are dissolved in a 0.05 M phosphate buffer (pH 6.5), stirred for one hr and shaken for two hrs. After one night, the solutions are filtered using a microtiter filter plate. Then the filtrate and its 1/10 dilution are analyzed by HPLC-UV. In addition, a four-point calibration curve is prepared from the 10 mM stock solutions and used for the solubility determination of the compounds. The results are in μg/mL. In case the percentage of sample measured in solution after evaporation divided by the calculated maximum of sample amount is bigger than 80%, the solubility is reported as bigger than this value.

Hepatocytes stability assay. Cryopreserved hepatocytes suspension was diluted to 2×10^6 viable cells/mL for human and 1×10^6 viable cells/mL for mouse in the incubation medium and transferred 50 μL into each well of 96-well plates. These plates were incubated at 37 ℃, 5% CO_2 with shaking at 900 rpm in the incubator. After 30-min pre-incubation, reactions were initiated by addition of 50μL of pre-warmed incubation medium containing 2 μM test compound to obtain a final compound concentration of 1 μM and a final cell density of 1×10^6 cells/mL for human and 0.5×10^6 cells/ml for mouse. After 2, 10, 20, 40, 60 and 120 minutes, 200 μL of ice cold acetonitrile containing an internal standard was added to terminate the reaction. Following precipitation and centrifugation, the amount of compound remaining in the samples were determined by LC-MS/MS.

Parallel Artificial Membrane Permeability Assay. The permeation of drugs is measured using a "sandwich" construction. Sample stock solution (DMSO) was diluted to 150 μM (DMSO%<2%) with donor buffer, and after the filtration the solution was added into donor plate. An acceptor plate coated with phospholipids (membrane) was placed onto the donor plate containing drug solution. Finally, the upper plate was filled with buffer solution. The donor concentration was determined at t-start as reference concentration. The drug concentrations in acceptor and donor plate were detected at t-end (~ 18 hrs). Donor buffer is 0.05 M MOPSO buffer at pH 6.5 with 0.5% (w/v) glyco cholic acid, acceptor buffer is 0.05 M MOPSO buffer at pH 6.5, and the membrane is 10% (w/v) egg lecithin with 0.5% (w/v) cholesterol in dodecane.

Plasma Protein Binding Assay. The determination of unbound compound is performed using a 96-well format equilibrium dialysis (HTDialysis, Gales Ferry, Connecticut, USA) with a molecular weight cutoff membrane of 12 to 14 kDa (HTDialysis, Gales Ferry, Connecticut, USA) and Diazepam used as positive controls. Pooled human and mouse plasma were purchased from Biopredic (Rennes, France). The equilibrium dialysis device itself is made of Teflon to minimize

non-specific binding of the test substance. For the HTD device, the dialysis membranes are conditioned as recommended by the supplier and the dialysis plate is assembled by placing conditioned membranes between rows of half-wells and tightly clamping the assembled apparatus. Compounds are tested in cassettes of 2-5 with an initial total concentration of 1000 nM, one of the cassette compound being the positive control. By determining the unbound fraction values for the positive control in each well, the integrity of membranes is tested. Equal volumes of matrix samples containing substances and blank dialysis buffer (Soerensen buffer at pH 7.4) are loaded into the donor and acceptor compartment respectively. The HTD dialysis block is sealed and kept for 5 hrs at a temperature of 37 °C and 5% CO_2 environment in an incubator. At the end of dialysis, the plasma and buffer samples were retrieved and the drug concentrations quantified by LC-MS/MS.

Pharmacokinetic (PK) Analysis. Compound was evaluated in female BALB/c mice (16–22 g. 12 mice in IV group were used for blood collection and 21 mice in PO group were used for blood and liver collection) at IV 1 mg/kg and PO 3 mg/kg. Compound was dissolved in 5% DMSO, 40% PEG400, 55% saline for i.v. dose and 2% Klucel, Tween 80, 0.1%Parabens in water for oral dose. Blood samples were collected at each time point and placed into tubes containing EDTA-K2 and centrifuged at 2000 g for 5 minutes at 4 °C to separate plasma from the samples. Following centrifugation, the resulting plasma was transferred to clean tubes and stored frozen in dry ice and then transferred into -80℃ fridge pending bioanalysis. Immediately after the collection of blood, liver samples of each animal in PO group will be harvested, rinsed with cold saline, dried with filter paper, and placed into a tube and weighed. Liver samples will be snap frozen in dry ice and then stored at -80 ℃ until bioanalysis. Plasma concentrations and liver concentration were

determined by LC–MS/MS, and the data were analyzed by a non-compartmental module of WinNonlin Professional v6.2. Any BLQs were omitted from the calculation.

In vivo Efficacy in HDI Mouse Model. The study was conducted by WuXi AppTec (Shanghai) Co., Ltd. All procedures in the study were in compliance with local animal welfare legislation, the Guide for the Care and Use of Laboratory Animals, and protocols approved by the WuXi AppTec (Shanghai) IACUC (Institutional Animal Care and Use Committee). Female BALB/c mice (6-8 weeks old) were injected through tail vein with 20 μg plasmid pcDNA3.1HBV encoding a 1.1-mer HBV genome (Genotype D) in a volume of normal saline equivalent to 8% of the mouse body weight. The total volume was delivered within a few seconds. 7 h post injection, mice were orally dosed by blank vehicle, 0.1 mg/kg of entecavir, or 3 mg/kg, and 12.5 mg/kg of **10** at indicated frequency for 5 days, respectively. Plasma and liver samples were collected at the indicated time points for HBV DNA quantification by real-time PCR.

CYP induction assay.

High throughput CYP induction screening assay. Cryopreserved hepatocytes were seeded on a 96-well collagen coated plate at a seeding density of 1×10^6 cells/mL. After 24 hrs culture in Williams E medium without serum, the test compounds at 0.1, 1.0, and 10 μM in serum-free culture media (0.1% DMSO content) were added in triplicates. A specific positive control inducer dependent on isoform (omeprazole for CYP1A2, phenobarbital for CYP2B6, or rifampicin for CYP3A4) was incubated alongside the test compounds. Negative control wells are also included on each plate consisting of vehicle alone (0.1% DMSO in Williams E media). Upon completion of the 24 hrs incubation, the hepatocytes are washed twice with Williams E media, and then lysed by adding 100 μL lysis binding solution. The lysates were stored at -80 °C until the qRT-PCR assay. Quantitative PCR analysis was performed on cDNA, using Applied Biosystems designed

TaqMan® gene expression assay for the target genes CYP1A2, CYP2B6, or CYP3A4. Peptidylprolyl isomerase A (PPIA) was used as a housekeeping gene. Samples were analyzed using an ABI 7900 HT real time PCR system. Relative fold mRNA expression levels of the target genes were determined based on the threshold cycle (CT) data of target genes relative to housekeeping gene for each reaction (DCT), normalized to the negative control (DDCT). Fold induction was calculated using the $2^{-\Delta\Delta CT}$ method. The cytotoxicity assays were not conducted, however, cell morphology during the test drug exposure period was monitored. Otherwise, a high CT number shift of PPIA from a baseline value of approx. 20 was considered as a consequence of cell toxicity indirectly indicated from this study.

Assay validation. The high throughput CYP induction screening assay was conducted for 24 hrs, which is shorter than the standard incubation time 48-72 hrs of a regulatory assay. Only one human liver donor was used to ensure detecting relatively strong positive induction flags. Positive induction signals of omeprazole (1, 10 and 100 microM) on CYP1A2 mRNA, phenobarbital (10, 100 and 1000 microM) on CYP2B6 mRNA, and rifampicin (0.1, 1 and 10 microM) on CYP3A4 mRNA could be obtained in a concentration-dependent manner. Internal historical data showed the mRNA fold induction of the positive control inducers at the highest concentrations was approximately >10, >2-6 and >10, respectively.

Ancillary Information

Supporting Information

The Supporting Information is available free of charge on the ACS Publications website.

X-ray structure of **(*S*)-19a**.

^{1}H-NMR, ^{13}C-NMR spectrums of **19.**

Molecular formula strings (CSV).

Corresponding author Information

*Wei Zhu (primary contact and paper writing): Phone: +86 21 28946743. Fax: +86 21 50790293. E-mail: wei.zhu.wz1@roche.com.

*Hong C. Shen: Phone: +86 21 28946738. E-mail: hong.shen.hs1@roche.com.

Wei Zhu and Hong C. Shen are the discovery chemistry project co-leaders.

Author Contributions:

Xianfeng Lin and Houguang Shi contributed equally to this work.

Acknowledgements

We are grateful to Qinshan Gao, Yang Lu, Wenzhi Cheng, Liqin Chen, Peilan Ding and Leimin Wang for the purification of final compounds and the analytical assistance. We thank the process group, including Jin She, Guocai Zhang and Junli Chen, for their assistance with large-scale synthesis campaigns. We thank Jieyu Dai and Kenichi Umehara for preparing the CYP induction assay protocol. We would like also thank André Alker for the analysis of the single crystal X-ray structure of **(*S*)-19a**.

This work was funded by F. Hoffmann-La Roche AG.

Abbreviations Used

HBV: hepatitis B virus; ADMET: absorption, distribution, metabolism, excretion and toxicity; HAP: heteroaryldihydropyrimidine; SAR: structure-activity-relationship; PK: pharmacokinetic; PD: pharmacodynamics; CYP: cytochromes P450; HBsAg: HBV surface antigen; PXR: pregnane X receptor; RIF: rifampicin; CSD: Cambridge structural database; SFC: supercritical fluid chromatography; HPLC: high performance liquid chromatography; PAMPA: parallel artificial membrane permeability assay; LYSA: lyophilisation solubility assay; PPB: plasma protein binding; SDPK: single-dose pharmacokinetics; HDI:, hydrodynamic injection; ETV: entecavir; hERG:

human ether-a-go-go-related gene; GSH: glutathione adduction; NOAEL: no observed adverse effect level.

References and Notes

Notes

The authors declare no competing financial interest.

All animal experiments performed in the manuscript were conducted in compliance with institutional guidelines.

References

(1) World Health Organization (WHO) Fact Sheet N°204,: http://www.who.int/mediacentre/factsheets/fs204/en/, accessed Apr.16, 2019.

(2) Feng, S.; Gao, L.; Han, X.; Hu, T.; Hu, Y.; Liu, H.; Thomas, A. W.; Yan, Z.; Yang, S.; Young, J. A. T.; Yun, H.; Zhu, W.; Shen, H. C. Discovery of small molecule therapeutics for treatment of chronic HBV infection. *ACS Infectious Diseases* **2018**, *4*, 257-277 and the references cited therein.

(3) Testoni, B.; Durantel, D.; Zoulim, F. Novel targets for hepatitis B virus therapy. *Liver Int.* **2017**, *37(S1)*, 33–39.

(4) Tang, L.; Zhao, Q.; Wu, S.; Cheng, J.; Chang, J.; Guo, J.-T. The current status and future directions of hepatitis B antiviral drug discovery. *Expert Opin. Drug Discovery* **2017**, *12*, 5–15.

(5) Deres. K,; Schröder, C. H.; Paessens, A.; Goldmann, S.; Hacker, H. J.; Weber, O.; Krämer, T.; Niewöhner, U.; Pleiss, U.; Stoltefuss, J.; Graef, E.; Koletzki, D.; Masantschek, R. N. A.; Reimann, A.; Jaeger, R.; Groβ, R.; Beckermann, B.; Schlemmer, K.-H.; Haebich, D.; Rübsamen-Waigmann, H. Inhibition of hepatitis B virus replication by drug-induced depletion of nucleocapsids. *Science* **2003**, *299*, 893–896.

(6) Qiu, Z.; Lin, X.; Zhang, W.; Zhou, M.; Guo, L.; Kocer, B.; Wu, G.; Zhang, Z.; Liu, H.; Shi, H.; Kou, B.; Hu, T.; Hu, Y.; Huang, M.; Yan, S. F.; Xu, Z.; Zhou, Z.; Qin, N.; Wang, Y. F.; Ren, S.; Qiu, H.; Zhang, Y.; Zhang, Y.; Wu, X.; Sun, K.; Zhong, S.; Xie, J.; Ottaviani, G.; Zhou, Y.; Zhu, L.; Tian, X.; Shi, L.; Shen, F.; Mao, Y.; Zhou, X.; Gao, L.; Young, J. A. T.; Wu, J. Z.; Yang, G.; Mayweg, A. V.; Shen, H. C.; Tang, G.; Zhu, W., Discovery and pre-clinical characterization of third-generation 4-H heteroaryldihydropyrimidine (HAP) analogues as hepatitis B virus (HBV) capsid inhibitors. *J. Med. Chem*. **2017**, *60*, 3352–3371.

(7) Zhou, S. F. Drugs behave as substrates inhibitors and inducers of human cytochrome P450 3A4. *Curr. Drug Metab.* **2008**, *9*, 310–322.

(8) Gao, Y.-D.; Olson, S. H.; Balkovec, J. M.; Zhu, Y.; Royo, I.; Yabut, J.; Evers, R.; Tan, E. Y.; Tang, W.; Hartley, D. P.; Mosley, R. T. Attenuating pregnane X receptor (PXR) activation: A molecular modelling approach. *Xenobiotica*, **2007**, *37*, 124-138.

(9) Sinz, M. W. Avoiding PXR and CAR activation and CYP3A4 enzyme induction. *Top. Med. Chem*. **2015**, *9*, 159–190.

(10) Groom, C. R.; Bruno, I. J.; Lightfoot, M. P.; Ward, S. C. The Cambridge structural database. *Acta Cryst*. **2016**, *B72*, 171-179.

(11) In vitro Metabolism and Transporter Mediated Drug-Drug Interaction Studies Guidance for Industry. https://www.fda.gov/downloads/Drugs/Guidances/UCM581965.pdf, accessed Apr.16, 2019.

(12) Nagai, M.; Konno, Y.; Satsukawa, M.; Yamashita, S.; Yoshinari, K. Establishment of in silico prediction models for CYP3A4 and CYP2B6 induction in human hepatocytes by multiple regression analysis using azole compounds *Drug Metab. Dispos*. **2016**, *44*, 1390-1398.

(13) Yang, P. L.; Althage, A.; Chung, J.; Chisari, F. V. Hydrodynamic injection of viral DNA: a mouse model of acute hepatitis B virus infection. *Proc. Natl. Acad. Sci. U. S. A*. **2002**, *99*, 13825–13830.

(14) Sells, M. A.; Chen, M. L.; Acs, G. Production of hepatitis B virus particles in HepG2 cells transfected with cloned hepatitis B virus DNA. *Proc. Natl. Acad. Sci. U. S. A.* **1987**, *84*, 1005-1009.

(15) Guo, H.; Jiang, D.; Zhou, T.; Cuconati, A.; Block, T. M.; Guo, J.-T. Characterization of the intracellular deproteinized relaxed circular DNA of hepatitis B virus: an intermediate of covalently closed circular DNA formation. *J. Virol.* **2007**, *81*, 12472-12484.

Table of Contents Graphic:

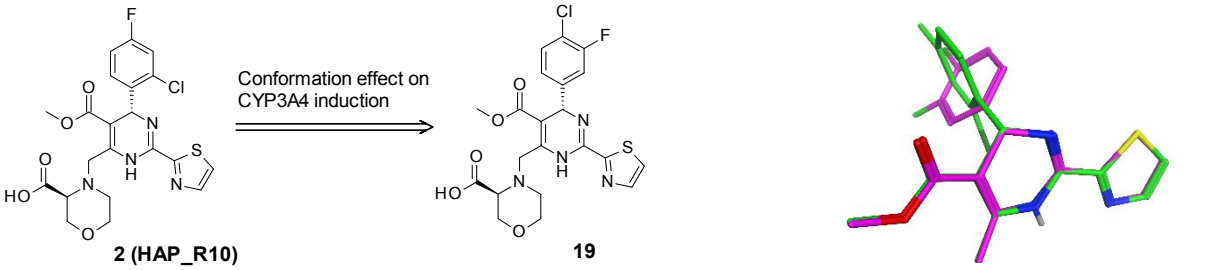

2 (HAP_R10)

EC_{50}/CC_{50}: 0.003 / >100 μM
CYP3A4 induction: 111% of rifampicin

19

EC_{50}/CC_{50}: 0.010 / >100 μM
CYP3A4 induction: 25% of rifampicin

Overlay of the cores of **2** and **19**
2: Green; **19**: Cyan